31st Congress of the International Council of the Aeronautical Sciences

Belo Horizonte, Brazil; September 09-14, 2018

SCALABLE DESIGN APPROACH TO ANALYZE FLIGHT MECHANICAL PERFORMANCE OF TILT-WING UAVS

Marten Schütt*, Tobias Islam*, Philipp Hartmann*, Dieter Moorman*
***Institute of Flight System Dynamics, RWTH Aachen University, Germany**

Keywords: *Tilt-wing, VTOL, UAV, Conceptual Design*

Abstract

This paper presents a method to evaluate different tilt-wing concepts for preliminary design. A separation of the aircraft into standardized components supports easy adaption and fast calculations, as all components have identical structure. Despite the flight mechanical complexity of tilt-wing aircraft, this method allows to keep the level of detail in the range of analytical or semi empirical equations with limited experimental data.

The component setup and implementation are presented as well as a method for flight mechanical analysis. Equations to calculate the forces and moments of each individual component are derived and discussed, whereby each component can consist of a propulsion unit, a wing and a flap. The effect of propeller slipstream on the wing aerodynamics are described in detail.

Results of the method in terms of different airfoils, flap deflections and thrust settings could be validated by wind tunnel measurements.

An exemplary tilt-wing aircraft is evaluated, presenting a possible application of the component buildup method. The special characteristics of the design of unconventional configurations are particularly emphasized regarding flight mechanics.

1 Introduction

Recent UAV designs try to bridge the gap between vertical take-off and landing (VTOL) and efficient cruise flight. Dependent on designated missions, the aircraft design has to set an optimal balance between efficiency during hover and cruise flight. Some aircraft in VTOL configuration use the same engines[1] for hover and cruise flight. This approach can be found in various UAVs like Germandrones Songbird [1], NASA GL-10 [2] but also in manned concepts like the Joby J2 [3]. Some UAVs have additional engines for hover, like Quantum Tron [4], AVIGLE tilt-wing [5] and DHL Pacelcopter [6]. A different approach is to have separate engines, designated for hover and cruise flight. This can also be found in UAVs, e.g. Airbus Quadcruiser [7] or Alti Transition [8].

For these configurations, the engines are either not efficient, as they are a trade-off between hover and cruise flight, or there must be more engines on board than necessary. The presented tilt-wing concept with a tiltable tailplane proposes a promising approach to compensate for this problem. This concept uses only three engines during hover, while one is designed for efficient and fast cruise flight.

The flight envelope of a convertible aircraft is extensive, combining characteristics and capabilities of rotorcraft with those of fixed-wing airplanes. The angel of attack (AoA) vary from $-180°$ to $+180°$ and the aerodynamic properties are highly nonlinear. Approaches to model convertible aircraft found in literature are extensive wind-tunnel tests ([9] and [10]), detailed computational fluid dynamics (CFD) analysis [3] or different approaches of vortex lattice methods [7].

[1] Engine is used in the following as a term for the combination of electric motor and propeller.

Apart from being expensive and time consuming, these approaches are very sensitive to changes of the configuration, which are likely during preliminary design phase. Instead an analytical and empirical model can be of high value for flight mechanical analysis. An analytic, component based description of aircraft was already used by Selig [11] for conventional aircraft. In literature different approaches for control design of unconventional UAVs can be found, whereby most of them are model-based. The applied models are often component based, in particular Tobing [12], Francenso [13] and Hartmann [14].

Within this paper a generic component buildup method (CBM) is presented that separates the aircraft into individual components. The forces and moments acting on each element are described by analytical and empirical calculations. Nevertheless, the basic aerodynamic and flight mechanical interactions are taken into account. The model is easily modifiable to evaluate different configurations and their varying flight mechanics. Within this model, the level of detail is kept appropriate for initial design and evaluation, but can be increased for selected sensitive effects or interactions.

This paper is structured as follows: In Sect. 2 the tilt-wing configuration including flight mechanics is presented, followed by a general introduction to the conceptual design approach (Sect. 3). In Sect. 4 all equations to evaluate the different components are presented, followed by a validation, using wind tunnel measurements (Sect. 5). In Sect. 6 an application of the method to analyze the flight mechanics of tilt-wing aircraft is presented.

2 Tilt-wing Configuration

The tilt-wing configuration combines advantages of rotary-wing and fixed-wing configurations. During cruise the wing is rotated to form a fixed wing configuration, producing sufficient lift. For hovering and VTOL the tilt-wing aircraft is able to rotate its wing around the lateral axis. As the main engines are installed on the wing, the thrust is used to compensate the weight of the aircraft.

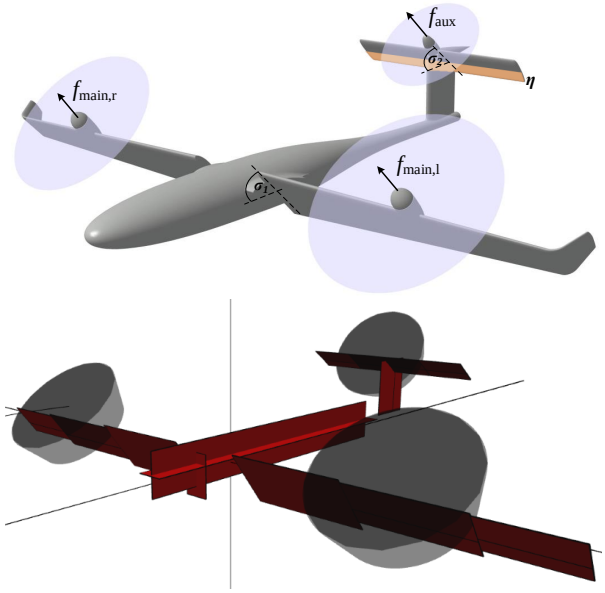

Fig. 1 Analyzed tilt-wing configuration with its longitudinal control devices (upper part) and separated into elements by the CBM (lower part)

The tilt-wing configuration includes all control surfaces typical to an fixed-wing aircraft. The ailerons are located in the slipstream of the propellers to gain yaw control in hover. To control pitching moment during hover an auxiliary engine is needed.

2.1 Analyzed Configuration

The presented tilt-wing concept includes a tiltable tailplane with an auxiliary engine mounted in front, see Fig. 1. During hover the two main engines produce most of the thrust while the auxiliary propeller mainly supports for pitch control. During cruise flight the main engines are switched off and the propellers folded away, while the auxiliary engine produces the thrust to compensate the drag of the aircraft. As the propellers of VTOL aircraft act in very different inflow conditions, the propeller design in general is a trade-off. For the analyzed configurations the propellers of the main engines can be designed to be efficient during hover while the propeller of auxiliary engine is efficient during cruise flight. This way the tilt-wing aircraft features efficient and fast cruise flight capabilities in

contrast to multirotor systems.

2.2 Flight Mechanics

During the transition from hover to cruise flight and vice versa a distinct assignment of control surface effects and the aircraft's rotational axis is not possible. Because of changing aerodynamics at different flight states, the actuators effectiveness varies in direction and magnitude. Dependent on a suitable choice of wing and engine, the tilt-wing aircraft can perform stationary flight within the entire flight envelope from hover to cruise. Stationary longitudinal flight conditions for all airspeeds over the entire flight envelope can be achieved by suitable trim control deflections and trim thrust settings. Dependent on the configuration, the number of trim control devices varies and thereby the dimension of the solution space of trim control deflections for each flight state. Considering the longitudinal motion, the presented configuration features the following control devices. The effect of one control device may be dependent on another (nonlinear behavior), e.g. as the engines are mounted on the wing/tailplane:

- main thrust: $f_{\text{main}} = f_{\text{main,r}} + f_{\text{main,l}}$
- auxiliary thrust: f_{aux}
- main tilt angle: σ_1
- tailplane tilt angle: σ_2
- elevator deflection: η

During conceptual design of tilt-wing aircraft, the design has to ensure that stationary flight within the entire flight envelope is possible.

3 Conceptual Design Approach

The CBM described in this paper is part of a generic simulation environment for analyzing flight mechanics and developing control algorithms, see Fig. 2 (adapted from Hartmann [14]). The CBM calculates the forces and moments on the aircraft based on control deflections, thrust settings and the current inflow. The forces and moments are used to evaluate the equations of motion, which describe rigid body motion [14]. The lateral, longitudinal and rotational motion of the aircraft results in a inflow condition. An existing wind model represents the motion of the atmosphere with respect to the inertial frame. Both motions amount to the total inflow. Controller commands are used in combination with actuator models to calculate control deflections. A detailed description of the simulation can be found in [14].

3.1 Objective

The analyzed tilt-wing configuration presents an approach to bridge the gap between flight performance and flight mechanical stability. Due to the wing and engine design, this configuration is more sensitive to effects of propeller slipstream on the wing and the wing downwash on the tailplane, compared to previously analyzed tilt-wing concepts. Smaller areas of the wing are influenced by the slipstream, which reduces the Reynolds numbers and therefore requires more detail in the description of the aerodynamics. The level of detail of the existing simulation is therefore increased for these effects.

The challenges of preliminary design of tilt-wing aircraft are quite different from those of fixed wing aircraft. Of course aerodynamic efficiency and lift-to-drag ratio during cruise are drivers, but the flight mechanical analysis over the entire flight envelope is also of high importance. This claims an appropriate description of the slipstream of the propeller as well as the description of the downwash of the wing affecting the tailplane. Considering these effects helps to analyze flight mechanics, especially the equilibrium of moments, with appropriate precision.

The goal of this CBM is to show the significant flight mechanical effects while being able to evaluate various different configurations in a short amount of time. The need of external data is limited to coefficients of the airfoils and thrust models of the engines. The adaption of different wings, propellers and overall geometry can be performed iteratively. This way it is possible to find an optimized configuration and analyze it for longitudinal motion.

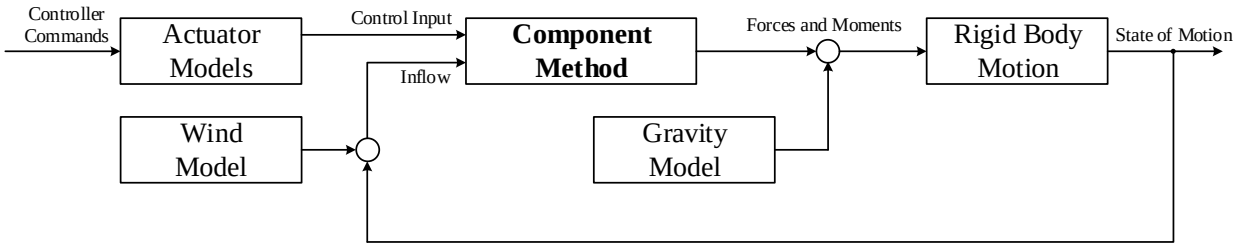

Fig. 2 The presented method, showing its input and output, embedded into an simulation environment, adapted from Hartmann [14]

3.2 Structure

As mentioned before, the presented CBM is part of a simulation environment. In this paper only the longitudinal motion is presented, neglecting any lateral flow. Key property of this method is the generic decomposition of the aircraft and the possibility to model all different parts by using the same component structure. Each component consists of a propeller disc, a wing element and a flap, see Fig. 3. The internal interaction of the different elements inside the component are considered, while all components are calculated individually without external interaction in the first place. Inside one component the impact of the propeller slipstream on the wing and the flap is considered by calculating individual inflow conditions. The size of one wing element is defined by the contracted propeller slipstream, see 4.1. For each component the aerodynamics are considered stationary. There are no iterative calculations, as for each timestep all elements are calculated unidirectional from nose to tail. The location and geometry of each component in terms of position and orientation as well as geometric parameters can be specified and each element (propeller, wing or flap) of a component can be omitted.

The calculation of each component is executed as follows. First the external inflow condition is used to calculate the thrust and slipstream of the propeller (Sect. 4.1). The slipstream and external inflow are used to calculate the lift, drag and moment of the wing element, dependent on

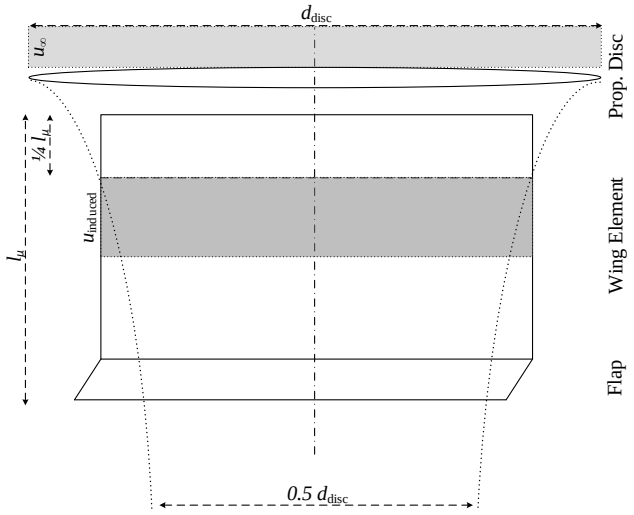

Fig. 3 The elements of the component and their inflow conditions.

the airfoil and flap deflection (Sect. 4.2). The entire lift distribution of the wing is used to calculate the downwash and its effect on the tailplane (Sect. 4.3).

To achieve an optimized tilt-wing configuration, different configurations can be trimmed using the CBM, for flight mechanical analysis (Sect. 6).

4 Implementation

The equations of motion refer to and the inflow conditions are calculated with respect to the CoG of the aircraft. The aircraft is divided into components that have a relative position to this reference system. Linear transformations can be used

to calculate the component's local inflow condition and the forces and moments acting on the CoG based on the component's local forces and moments [14]. Transformations are dependent on relative position between CoG and component only.

4.1 Propeller Disc and Slipstream

The propeller control input for each component is static thrust, as the effective thrust is dependent on the local inflow condition, which is calculated for each element individually. Actuator models describe the correlation between throttle and static thrust of each engine. The propeller diameter (d_{disc}) and the distance of the propeller disc to the aerodynamic center of the wing are necessary geometry information. In general the calculations consists of the following steps:

- Reduce the static thrust due to the local inflow condition
- Calculate the slipstream of the propeller by momentum theory
- Reduce the induced velocity by use of contraction and continuity equation

The correlation between static (f_0) and effective thrust ($f_{\text{effective}}$), dependent on the current axial inflow (u_∞), is different for each propeller. Therefore it is based on experimental measurements.

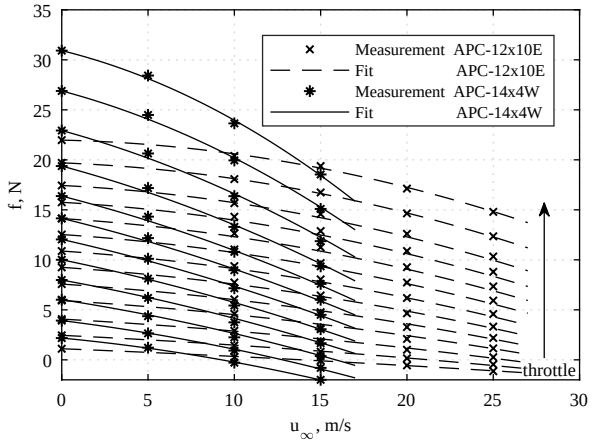

Fig. 4 Measurement data and quadratic fit results of two different APC-Propellers.

Fig. 4 shows wind tunnel data of the correlation between effective thrust and axial inflow for two different propellers. For the CBM these data are approximated by a quadratic function (with parameters a_{11} to a_{23}), see Equ. 1. Thanks to this relationship, the effective thrust can be calculated dependent on the current axial inflow:

$$\begin{aligned} p_1 &= a_{13} \cdot {f_0}^2 + a_{12} \cdot f_0 + a_{11} \\ p_2 &= a_{23} \cdot {f_0}^2 + a_{22} \cdot f_0 + a_{21} \\ f_{\text{effective}} &= p_1 \cdot {u_\infty}^2 + p_2 \cdot u_\infty + f_0 \end{aligned} \tag{1}$$

The average slipstream velocity ($\bar{u}_{\text{contr}}$) of the propeller is calculated by using momentum theory, see Equ. 2. The velocity is calculated for the fully contracted slipstream in the far-field of the propeller. Therefore the induced part of the velocities has to be corrected by transferring it to the aerodynamic center $\left(x_{\text{chord}} = \frac{1}{4} l_\mu\right)$ of the wing, by using the contraction factor (k_d) of a slipstream (see Equ. 3 from [15]). The dynamic pressure of the wing, as sum of induced and freestream velocity, can be used to calculate lift and drag, see Fig. 3.

$$\bar{u}_{\text{contr}} = \sqrt{\frac{2 \cdot f_{\text{effective}}}{\rho \cdot A_{\text{disc}}} + {u_\infty}^2} \tag{2}$$

$$k_d = 1 + \frac{x_{\text{chord}}}{\sqrt{{x_{\text{chord}}}^2 + \left(\frac{d_{\text{disc}}}{2}\right)^2}} \tag{3}$$

4.2 Wing Element

The geometry, the airfoil and the inflow condition, in terms of dynamic pressure ($\bar{q}$), AoA and Reynolds-Number (Re), of the wing is known. These data are used to calculate the aerodynamic forces of the wing element. The polars of the coefficients (c_l, c_d, c_m) of each airfoil have to be precalculated, e.g. by use of *xfoil* [16]. Usually the polars calculated by *xfoil* are valid in a maximum range of AoA from $-10°$ to $+20°$. For VTOL aircraft this is insufficient, as the inflow might come from any direction. Therefore the polars are extrapolated by use of the Montgomerie approach [17]. In Fig. 5 the calculated and extrapolated polars for two airfoils are shown.

The calculation of the currently acting forces and moments of the wing element consists of the following steps:

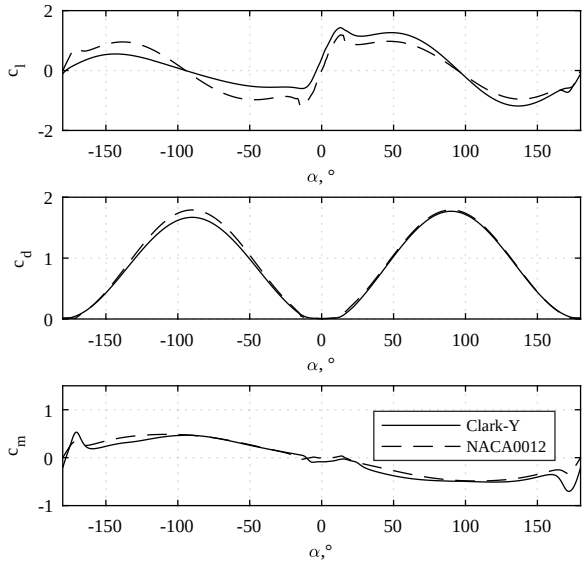

Fig. 5 Extrapolated polars of *Clark-Y* and *NACA0012* airfoil for Re = 450,000.

- Identify the current AoA and *Re* of the wing element
- Look up the current corresponding aerodynamic coefficients
- Calculate the change of the aerodynamic coefficients due to flap deflection
- Reduce the lift coefficient for the finite wing
- Calculate the induced drag for the finite wing
- Calculate the pitching moment coefficient for the finite wing
- Calculate the forces and moments

As we only investigate the longitudinal motion, all crossflow and side slip angles are neglected. This means the current AoA is simply $\alpha = arctan\left(\frac{w_\infty}{u_{chord}}\right)$ and the Reynolds number $Re = \frac{l_\mu \cdot \sqrt{{w_\infty}^2 + {u_{chord}}^2}}{\nu}$. As these aerodynamic coefficients are valid for airfoils of infinite span and no flap deflection, they have to be modified to finite wing coefficients (c_L, c_D, c_M). These coefficients are finally applied to calculate the current lift, drag and pitching moment. In combination with the thrust these are transfered into the element coordinate system to obtain the acting forces and moments for each element.

4.2.1 Flap Deflection

The effect of flap deflection is represented by manipulation of the aerodynamic coefficients of the airfoil. Thereby change of lift, drag and moment is taken into account. Equ. (4) and (5) are derived from Datcom [18]. This approach is suitable for plain flaps ([18]), which are commonly used in UAVs as ailerons and elevator.

$$\frac{\delta c_l}{\delta \kappa} = \chi_{d1} \cdot \chi_{d2} \cdot \eta_d \cdot cos(\alpha) \tag{4}$$

$$\frac{\delta c_m}{\delta \kappa} = \frac{\delta c_l}{\delta \kappa} \cdot 0.25 \cdot (\lambda - 1) \cdot cos(\alpha) \tag{5}$$

The empirical factors $\chi_d 1$ and $\chi_d 1$ are approximated linear and quadratic dependent on the flap to chord ratio λ.

$$\chi_{d1} = -5.56 \cdot \lambda^2 + 11.39 \cdot \lambda + 1.54 \tag{6}$$

$$\chi_{d2} = 0.36 \cdot \lambda + 0.36 \tag{7}$$

The non-linear effect of greater deflection angles ($> 12°$) is represented by the factor η_d, quadratic dependent on the deflection angle κ in radiant.

$$\eta_d = \begin{cases} 1 & \text{for } \kappa \leq 12° \\ 0.822 \cdot \kappa^2 - 1.73 \cdot \kappa + 1.35 & \text{for } \kappa > 12° \end{cases} \tag{8}$$

The effect of drag due to flap deflection is partial represented by increasing the induced drag, as mentioned in the next section. Additionally Equ. 9 was derived from empirical analysis using *xfoil*, as in literature the impact of flap deflection on drag is not discussed. Observed nonlinear effects for high AoA were implemented for all coefficient by trigonometric functions of AoA and deflection angle.

$$\delta c_d = 0.33 \cdot \delta\kappa^2 + 0.35 \cdot \sin(\alpha) \cdot \tan(\delta\kappa) \tag{9}$$

4.2.2 Lift of the Wing Element

The finite wing causes loss in lift compared to an airfoil of infinite span. Equ. 10, from [19], describes the reduction of the linear slope of the lift coefficient from an airfoil to a finite wing dependent on the aspect ratio (*AR*). This equation is applied for the entire AoA and not only for the linear region of the polar. The *AR*, applied for lift reduction in Equ. (10), represents the entire wing,

independent of the dimensions of the single components. The tailplane and fin are treated equally as wings, as long as it is a fuselage mounted configuration. The analyzed aircraft features a T-tail and the geometric AR of the fin is therefore modified by $AR_{corr} = 1.9 \cdot AR_{geo}$, from [18].

$$c_{L\alpha} = c_{l\alpha} \cdot \frac{AR}{\sqrt{AR^2+4}+2} \tag{10}$$

4.2.3 Drag of the Wing Element

The drag of a wing element on the one hand consists of the friction-drag and the form-drag, which is already considered in the drag polar of *xfloil*. On the other hand, the generation of lift produces a downwash, which induces another form of drag, that has to be added. The relationship of lift and induced drag is quadratic, see Equ. 11 ([19]).

$$c_D = c_d + \frac{{c_L}^2}{\pi \cdot AR \cdot e} \tag{11}$$

The Oswald-Factor e is calculated by semi-empiric Equ. 12 ([20]).

$$e = \frac{2}{2 - AR + \sqrt{4+AR^2}} \tag{12}$$

Additional aircraft drag like fuselage, nacelle or interference drag is summed up into a drag-plate, an element without flap or engine, see Fig. 1. This element is of a certain size, to obtain a suitable drag force.

4.2.4 Moment of the Wing Element

The pitching moment coefficient calculated by *xfoil* is referred to the $\left(\frac{1}{4}l_\mu\right)$ line. The coefficient describes the shift of the center of pressure (CoP) on the airfoil in combination with the de- or increase of the lift coefficient. The variation of the lever arm and force influences the moment regarding the $\left(\frac{1}{4}l_\mu\right)$ line for different AoA. As the reference point of the component itself is on the $\left(\frac{1}{4}l_\mu\right)$ line, no transformation is necessary. Montgomery gives an equation to calculate the CoP in reference to the leading edge (LE) for an airfoil,

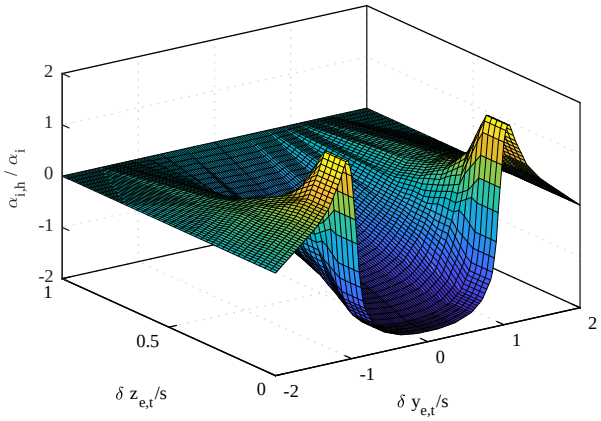

Fig. 6 Change of AoA of the tailpane due to downwash as function of position $\delta y_{e,t}/s$ and $\delta z_{e,t}/s$, extrapolated from [21].

see Equ. 13 ([17]).

$$arm = \frac{c_m|_{\left(\frac{1}{4}l_\mu\right)}}{-c_l \cdot \cos(\alpha) - c_d \cdot \sin(\alpha)} + 0.25 \tag{13}$$

For any inflow condition, in combination with the airfoil polars, the location of the CoP (arm) can be calculated. The CoP is assumed identically for the finite wing. By Equ. 14 the pitching moment coefficient (c_M) of the wing can be calculated thanks to the previously determined coefficients (c_L, c_D).

$$c_M|_{\left(\frac{1}{4}l_\mu\right)} = (-c_L \cdot \cos(\alpha) - c_D \cdot \sin(\alpha)) \cdot (arm - 0.25) \tag{14}$$

4.3 Wing Downwash

The impact of the wing on the empennage is mainly a change in AoA of the tailplane due to downwash (w_i) of the wing [19]. According to [14] this effect is essential, as it influences the pitching moment and changes significantly for different tilt-angles of the wing. The downwash is created by the vortex system of the wing. The magnitude of the effect is dependent on the lift of the wing, the span of the tailplane and the relative position between wing and tailplane.

Glauert [21] describes a theoretical downwash distribution for the three dimensional farfield of the wing. Dependent on the location

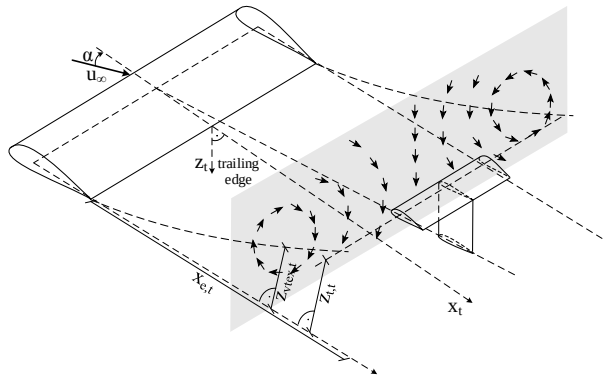

Fig. 7 Geometric relation of wing, tailplane and vortex system

of the tailplane, the relation $\left(\frac{\alpha_{i,tail}}{\alpha_i}\right)$ of the induced AoA of the wing (α_i) and the downwash AoA at the loaction of the tailpane $(\alpha_{i,\text{tail}})$ can be calculated from these data. The relative position is given in terms of the half span s. The distribution was inter- and extrapolated to use it for the geometric correlations of tilt-wing UAV, see Fig. 6. The downwash distribution was calculated for a wing with an elliptical lift distribution, but they are also applicable for wings with different lift distributions, in particular trapezoidal wings [19]. In Fig. 7 the geometric relations of wing, vortex system and tailplane are described. The induced AoA of the wing $\left(\alpha_i = \frac{c_{L\text{wing}}}{\pi \cdot AR}\right)$ is derived from the lift coefficient of the entire wing, including propeller induced lift, $\left(c_{L\text{wing}} = \frac{2 \cdot L_{\text{wing}}}{\rho \cdot u_\infty \cdot A_{\text{wing}}}\right)$. The downwash ($w_{\text{induced}} = \alpha_{i,tail} \cdot u_{\text{wing}}$, for small $\alpha_{i,tail}$) is finally added to the undisturbed inflow of the tailplane. This way the inflow condition of all components located behind the wing can be calculated.

5 Validation

Some of the analytical and semi-empirical equations could be validated by wind tunnel measurements. Wings of different geometries and with different airfoils were analyzed for various inflow conditions. Additionally the effect of flap deflection and propeller interaction on the aerodynamic coefficients are presented. All measurements were performed in a Göttingen-type wind tunnel using a 6-components-gauge to measure forces and moments. The parameters of the analyzed wings are varying in geometry, airfoil and inflow condition, as the measurements were not performed exclusively to validate this approach. Wings corresponding to the measurement data were modeled by the CBM for the given inflow condition.

5.1 Wind Tunnel Measurements

Two clean rectangular wings with an AR of 4.2 are analyzed featuring two different airfoils, *Clark-Y* and *NACA0012*. Both were analyzed for a Re of 402,000 including AoA from $-3°$ to $15°$.

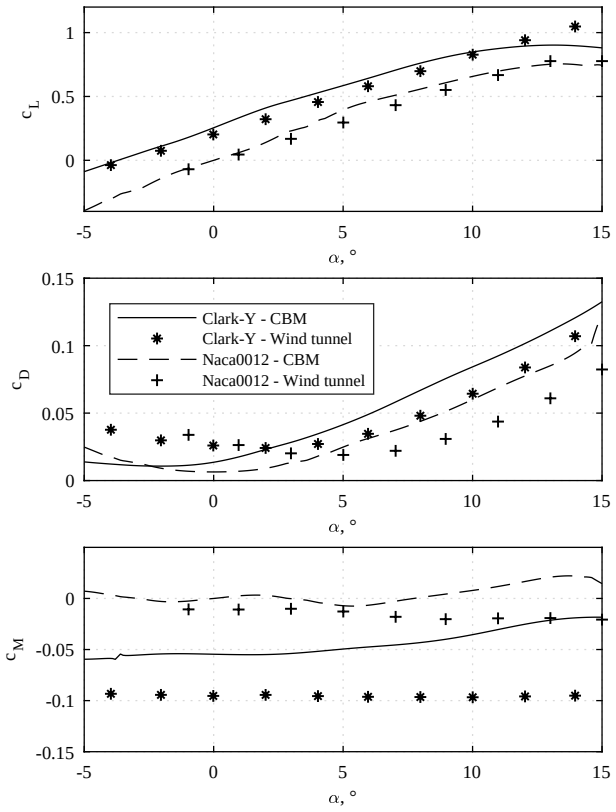

Fig. 8 Comparison of wind tunnel measurements and simulation of a rectangular wing of $AR = 4.2$ with *Clark-Y* and *NACA0012* airfoil for Re = 402,000

In Fig. 8 the aerodynamic coefficients of both wings are presented. The wind tunnel measurement shows a linear relation of c_L and α for both wings up to $15°$. The CBM reduces the lift polar

of the airfoil which results in an overestimation of c_l between AoA of 0° and 10°. For higher AoA the slope of c_L of the CBM decreases, representing stall. This behavior can not be found for neither of both wings in the wind tunnel measurements. As stall is expected to occur for the wind tunnel for slightly higher AoA, it is not assumed that the error will increase by much for higher AoA.

The zero lift drag is underestimated by the CBM for both wings likely. For higher AoA the total drag coefficient c_D increases more than the wind tunnel measurement shows, which results in an maximum error by overestimation for both wings at AoA of around 9°.

The wind tunnel measurements show a approximately constant c_M for both wings for the entire AoA range. The CBM calculates a constant c_M up to 10°, the coefficient of *NACA0012* airfoils fits the measurement very well. The wrong stall characteristics of the CBM increases the error in moment for both wings for higher AoA.

Another wing of the airfoil *NACA0012*, which is equipped with a trailing edge flap of 35% chord, was analyzed in the wind tunnel for Re of 100,000. The AR is 5.2 and the flap was deflected ±20° and ±10°. In Fig. 9 the change of the aerodynamic coefficients due to flap deflection is presented for AoA from 0° to 90°. The effect in change of lift is very constant for AoA from 0° to 20° and decreases for higher AoA. This is estimated by the CBM very well, except for the stall region around $\alpha = 23°$. The effect in drag shows greater deviations to the measurement, again especially for AoA in the stall region. Nevertheless, asymmetric effects between positive and negative flap deflections are represented by the CBM. The constant change in moment (except for the stall region) for the entire range of AoA, is estimated by the CBM with small deviations.

A wing with an AR of 5.2 and a *NACA0012* airfoil, which was equipped with a propeller in front of it, was analyzed in the wind tunnel. The propeller is an *APC12x10E*, which was mounted 6 cm in front of the LE of the wing, producing

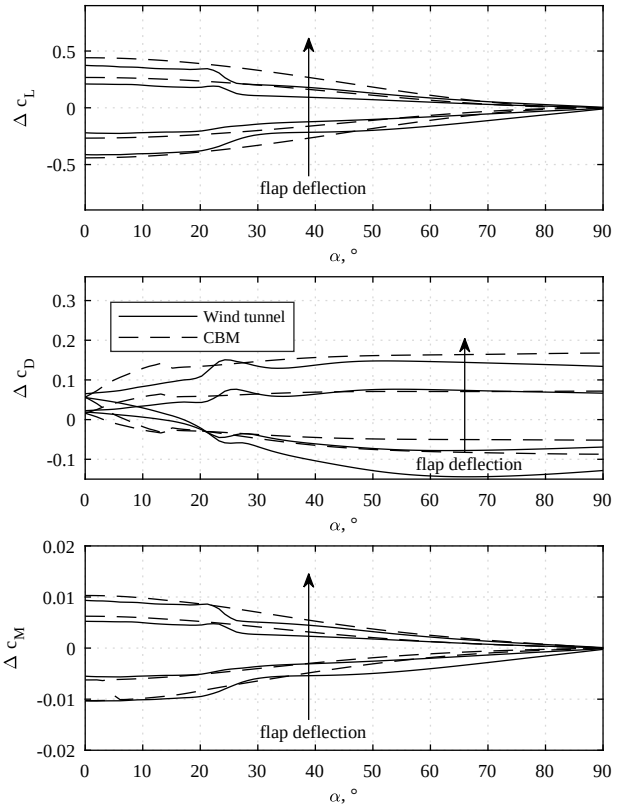

Fig. 9 Effect of flap deflection ($-20°, -10°, +10°, +20°$) for a rectangular wing of $AR = 5.2$ with *NACA0012* airfoil for $\lambda = 0.35$ for Re = 100,000

5 *N* and 10 *N* static thrust. The freestream Re was 67,000, not including the downwash of the propeller. In Fig. 10 the change of the aerodynamic coefficients due to thrust settings is presented. The effect in change of lift is overestimated by the CBM for both thrust settings for AoA up to $\approx 27°$. The change in drag is negative and decreasing for higher AoA, as the thrust acts in the opposite direction of the drag for an AoA of 0. The trend of the change in c_D is estimated by the CBM very well. The expected change in moment due to thrust is very low, as the engine is mounted coaxial to the chord of the symmetric wing. The CBM estimates similar, very low change of pitching moment.

5.2 Evaluation

The CBM estimated the trend for all coefficients of the entire analyzed AoA range. The most ob-

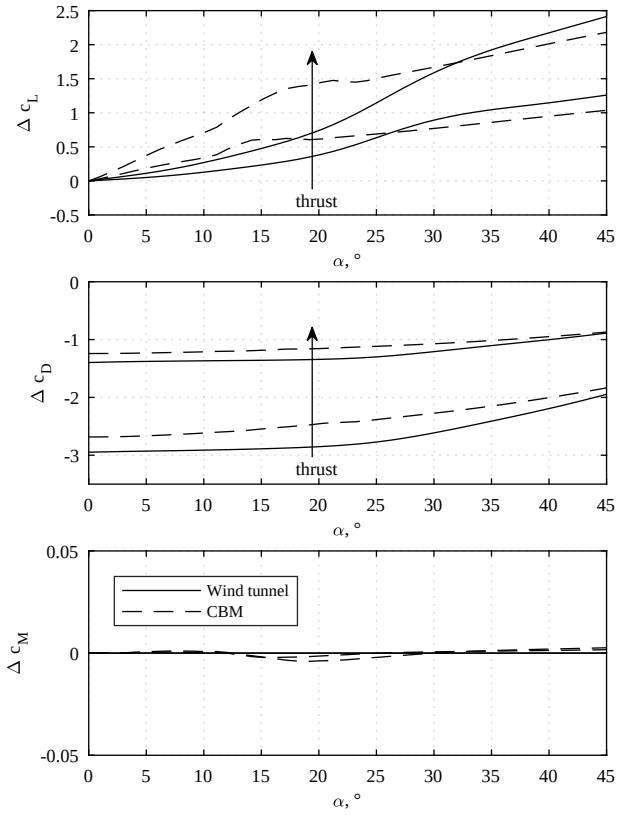

Fig. 10 Impact of propeller downwash (engine with $d_{\text{disc}} = 0.3m$ producing $5N$ and $10N$ thrust) for a rectangular wing of $AR = 5.2$ with *NACA0012* airfoil for freestream Re = 67,000

vious deviations occur in the stall region, which have to be analyzed and modeled in greater detail. Also the zero lift drag needs to be increased from airfoil to finite wing. Significant differences between airfoils as well as due to flap deflection could be observed and represent the measurements very well. The lift due to thrust shows significant deviations, again in the area of stall.

Comparing the effects of deviations in pitching moment coefficient to the occurring moments of the entire aircraft, shows only minor effects in the equilibrium of moments.

The applied general airfoil polars and equations for finite wings are not direct applicable to wings off small UAVs and low Re. Nevertheless, the flight mechanics for initial aircraft and controller design are represented adequate.

The effect of wing downwash on the empennage could not be validated in detail, but the occurring AoA are physically plausible.

6 Flight Mechanical Analysis

In the following an exemplary application of the CBM is presented. For a tilt-wing aircraft with given requirements, the procedure to design a suitable wing is presented. Despite the simple approach to calculate drag and lift, significant differences between airfoils and wing geometry can be identified. The aircraft requirements like cruise-speed, mass, engine and empennage are determined in the following section, additional to boundaries for the variable wing parameters, like span, airfoils chord-width. Each set of requirements and parameters defines an unique aircraft with different geometry, lever arms and wing. All aircraft have to be analyzed for their stationary cruise flight but additionally for their flight mechanics in the entire flight envelope.

6.1 Requirements

The following parameters state aircraft requirements, which need to be derived from the mission. The maximum takeoff mass and the design cruise speed are most relevant for the design of the wing. Next to cruise flight, the location of CoG and engines are very much dependent on flight mechanics during hover. In this case the empennage, in terms of lever arm, airfoil and size, is designed based on flight mechanical considerations, which are not part of this paper. The fixed parameters defining the aircraft are:

- u_{cruise}: Design cruise speed, most relevant for wing design.
- Total mass: The entire aircraft is summed up into a point mass, as the elements are weightless.
- CoG: In distance behind wing LE, may be dependent on the current tilt angle.
- Moment of inertia: Based on an estimated mass distribution in reference to the CoG.
- $D_{fuselage}$: Drag plate of a size to compensate for all interference/parasitic drag.

The parameters characterizing a trapezoidal wing are summed up in Tab. 1. The boundaries

were set by aerodynamic considerations. The tip chord must not fall below 0.1 m, maintaining a minimum *Re*, as polars for very low *Re* are hard to derive. Speed and size of the aircraft lead to airfoils for low *Re* performance, which were chosen from *UIUC database* [22].

Table 1 Parameters defining the Wing Components

Parameter	min	max
span	1.0 m	2.0 m
c_{root}	0.2 m	0.4 m
c_{tip}	0.1 m	0.3 m
airfoil	*Göttingen GOE-398, Clark-Y Selig S-2027, Eppler E434 Wortmann FX 84-W-140*	

6.2 Flight Mechanics

The flight mechanics of all configurations have to be analyzed for the flight envelope from hover to cruise speed. Trimmed flight states should be satisfied by all configurations due to the number of control variables. The state variables of the longitudinal motion are:

- position: x, z
- airspeed: u, w
- attitude angle: θ
- angular velocity: q

In consideration of trimmed flight states, the angular velocity q is zero and the positions x and z are irrelevant. Thanks to the number of control variables, the three remaining state variables (speeds u, w, and pitch angle θ) can be chosen freely within the flight envelope, while remaining the equilibrium of forces and moments.

6.3 Application

For each of the possible configurations, a model of the aircraft was set up using the CBM. The configurations were then trimmed for stationary flight for the entire flight envelope. A nonlinear numerical method[2] is used to minimize the remaining horizontal and vertical forces (X and Z) and the pitch moment (M), by actuator deflection and thrust setting. This states a multidimensional, nonlinear problem.

6.3.1 Wing Design

The analysis for an optimal wing focuses on level cruiseflight ($u = u_{\text{cruise}}$ and $w = 0$) and a horizontal fuselage ($\theta = 0$). The chosen actuators to trim the aircraft during cruise are the tilt angle of the wing and tailplane and the thrust of the tail engine. The effect of the main engines is neglected as the propellers are folded away during cruise flight. This way the nonlinear problem reveals a unique solution.

Each trimmed configuration creates the same amount of lift-force, but wing and tailplane induce different amount of drag-force. Therefore, the configurations equipped with a different wing, can be ranked by lift-to-drag ratio. The lift-to-drag ratio (Equ. 15) also takes fixed drag from the fuselage etc. and drag due to trim defections to achieve trimmed flight state into account.

$$\gamma_{\text{ac}} = \frac{m \cdot g}{D_{\text{wing}} + D_{\text{empennage}} + D_{\text{fuselage}}} \tag{15}$$

6.3.2 Flight Envelope

For each configuration all combinations of horizontal and vertical speed of the flight envelope have to be analyzed. Again, the fuselage should be horizontal, but the number of actuators to trim the aircraft during hover and transition to cruise flight increases to four: Tilt angle of wing (σ_1) and tailplane (σ_2), thrust of main (f_{main}) and tail (f_{aux}) engine. This way the multidimensional, nonlinear problem doesn't reveal a unique solution but requires additional boundaries or weighing functions. A possibility to compare all different solutions are the following properties:

- **Max. Acceleration**: Assuming limited control speed of all control variables, the gradient of corresponding trim control deflections between two flight states limits the flight state transition velocity.
- **Controllability**: Each control variable has a limited deflection. The trim deflection

[2] *The Mathworks Matlab* - fminsearch

reduces the remaining deflection available for steering.

- **Robustness**: Each set of trim control deflection is differently sensitive to errors in trim-state (velocity, attitude), resulting in unintended accelerations.

A possible weight function, making these properties comparable to analyze the flight mechanical performance, is dependent on the mission. An optimization concerning flight mechanics may reduce the cruise flight performance by far. As the CBM is designed to mimic the flight mechanics of tilt-wing UAVs, it is a powerful tool to find the optimal compromise.

7 Conclusion and Future Work

This analysis aims to explore the general applicability of the CBM for preliminary design of tilt-wing UAVs. A possibility to model each component of a tilt-wing aircraft in terms of aerodynamics and flight mechanics was presented. A level of detail was proposed, keeping the experimental or empirical data to a minimum, while the possibility to add detailed information is provided.

The setup of the method, especially the decomposition of the aircraft into components of identical structure was described. The components are able to model all essential parts of a tilt-wing aircraft and can consist of a propulsion unit, a wing element and a flap. The equations to calculate the forces and moments of all components of the aircraft were presented. While deriving the relations, a focus was set on the description of the effect of the propeller slipstream and flap deflection.

A validation by wind tunnel measurements shows that effects of different airfoil, flap deflection and thrust setting are represented by the CBM. Despite deviations in zero-lift-drag and stall characteristics, all significant effects of the flight mechanics are depict for initial design.

An application to analyze the flight mechanics of tilt-wing aircraft was presented. Based on an example configuration, the necessary requirements of the method were discussed. Finally a procedure to interpret the results of the method for wing design and trimmed flight states could be described.

While existing deviations of stall characteristics are state of current improvements, a validation of the complete model, including the effect of wing downwash on the empennage, is still to be made.

Contact

M. Schütt: schuett@fsd.rwth-aachen.de

References

[1] https://www.germandrones.com/

[2] Fredericks, W. J.; Moore, M. D.; Busan, R. C.: Benefits of hybrid-electric propulsion to achieve 4x increase in cruise efficiency for a VTOL aircraft. *AIAA International Powered Lift Conference, AVIATION Forum*, American Institute of Aeronautics and Astronautics, (2013). https://doi.org/10.2514/6.2013-4324

[3] Stoll, A.M; et al.: Conceptual Design of the Joby S2 Electric VTOL PAV. *14th AIAA Aviation Technology, Integration, and Operations Conference*, Atlanta, US-GA, (2014).

[4] https://www.quantum-systems.com

[5] Holsten, J.; Ostermann, T.; Moormann, D.: *Design and wind tunnel tests of a tiltwing UAV*. CEAS Aeronautical Journal Jg. 2, Nr. 1/4, S. 69-79, (2011).

[6] Schütt, M.; Hartmann, P.; Holsten, J.; Moormann, D.: *Mission Control Concept for Parcel Delivery Operations based on a Tiltwing Aircraft System*. 4th CEAS Specialist Conference on Guidance, Navigation & Control, Warsaw, Poland, (2017).

[7] Haimerl, M.; Binz, F.; Engels, S.; Moormann, D.: Entwicklung einer modifizierten, instationären Wirbelgittermethode für eine senkrechtstartfähige Flugzeugkonfiguration. *Deutscher Luft- und Raumfahrtkongress*, Deutsche Gesellschaft für Luft- und Raumfahrt - Lilienthal-Oberth e.V, (2017).

[8] https://www.altiuas.com/

[9] Rothhaar, P. M. et al.: NASA Langley Distributed Propulsion VTOL Tilt-Wing Aircraft

Testing, Modeling, Simulation, Control, and Flight Test Development. *14th AIAA Aviation Technology, Integration, and Operations Conference*, Atlanta, US-GA, (2014).

[10] Schütt, M.; Hartmann, P.; Moormann, D.: Fullscale Windtunnel Investigation of Actuator Effectiveness during Stationary Flight within the Entire Flight Envelope of a Tilt-wing MAV. *International Micro Air Vehicle Conference and Competition*, Delft University of Technology, (2014).

[11] Selig, M. S.: Modeling Full Envelope Aerodynamics of Small UAVs in Real Time. *AIAA Atmospheric Flight Mechanics Conference*, AIAA Paper 2010-7635, (2010). https://doi.org/10.2514/6.2010-7635

[12] Tobing, S.; Go, T. H.; Vasilescu R.: Improved Component Buildup Method for Fast Prediction of the Aerodynamic Performances of a Vertical Takeoff and Landing Micro Air Vehicle. *Computational Fluid Dynamics*, pp 209-214, (2008).

[13] Di Francesco, G.; Mattei, M.: Modeling and incremental nonlinear dynamic inversion control of a novel unmanned tiltrotor. *Journal of Aircraft*, Jg. 53, Nr. 1, S. 73-86, (2015).

[14] Hartmann, P.: *Predictive Flight Path Control for Tilt-Wing Aircraft*. Dissertation, RWTH Aachen, (2017).

[15] McCormick, B. W.: *Aerodynamics, Aeronautics, and Flight Mechanics*. Wiley, New York, (1994).

[16] Drela M.: *XFOIL: An Analysis and Design System for Low Reynolds Number Airfoils*. Low Reynolds Number Aerodynamics. Lecture Notes in Engineering, Springer, Berlin Heidelberg, (1989).

[17] Montgomerie, B.: *Methods for root effects, tip effects and extending the angle of attack range to +/-180, with application to aerodynamics for blades on wind turbines and propellers*. Swedish Defence Research Agency, (2004).

[18] Hoak, D.E.; Finck, R.D.: *USAF Stability and Control Datcom*. Flight Control Division, Air Force Flight Dynamics Laboratory, Wright-Patternson Air Force Base, Ohio, (1978).

[19] Schlichting, H.; Truckenbrot, E.: *Aerodynamik des Flugzeuges*. Springer, Berlin Heidelberg, (2001).

[20] Brandt, S.A.; et al.: *Introduction to Aeronautics: A Design Perspective*. AIAA Education Series, AIAA Inc., Washington, (2004).

[21] Glauert, H.: *The Elements of Aerofoil and Airscrew Theory*. Cambridge Science Classics, Cambridge University Press, Cambridge(1983).

[22] Williamson, G.A.; et al.: *Summary of Low-Speed Airfoil Data Vol. 5*. Department of Aerospace Engineering, University of Illinois at Urbana-Champaign, Urbana, (2012).

Copyright Statement